Observations of Ship Tracks from Ship-Based Platforms

W. PORCH,* R. BORYS,+ P. DURKEE,# R. GASPAROVIC,@ W. HOOPER,& E. HINDMAN,** AND K. NIELSEN#

* *Los Alamos National Laboratory, Los Alamos, New Mexico*
+ *Atmospheric Sciences Center, Desert Research Institute, Reno, Nevada*
# *Department of Meteorology, Naval Postgraduate School, Monterey, California*
@ *The Johns Hopkins University, APL, Laurel, Maryland*
& *Naval Research Laboratory, Washington, D.C.*
** *Earth and Atmospheric Sciences Department, City College of New York, New York, New York*

(Manuscript received 17 October 1997, in final form 17 February 1998)

ABSTRACT

Ship-based measurements in June 1994 provided information about ship-track clouds and associated atmospheric environment observed from below cloud levels that provide a perspective different from satellite and aircraft measurements. Surface measurements of latent and sensible heat fluxes, sea surface temperatures, and meteorological profiles with free and tethered balloons provided necessary input conditions for models of ship-track formation and maintenance. Remote sensing measurements showed a coupling of ship plume dynamics and entrainment into overlaying clouds. Morphological and dynamic effects were observed on clouds unique to the ship tracks. These morphological changes included lower cloud bases early in the ship-track formation, evidence of raised cloud bases in more mature tracks, sometimes higher cloud tops, thin cloud-free regions paralleling the tracks, and often stronger radar returns. The ship-based lidar aerosol measurements revealed that ship plumes often interacted with the overlying clouds in an intermittent rather than continuous manner. These observations imply that more must be learned about ship-track dynamics before simple relations between cloud condensation nuclei and cloud brightness can be developed.

1. Introduction

Ship-track clouds were first described by Conover (1966) as anomalous cloud lines observed in satellite images. These cloud lines can extend for hundreds of kilometers and persist for several days. Multiple observations made from a small research vessel (R/V *Glorita*) during the Monterey Area Ship Tracks (MAST) experiment in June 1994 are combined to describe the physical and dynamic characteristics of ship-track clouds. A wide variety of aerosol and meteorological parameters were simultaneously measured from the R/V *Glorita* with aircraft flights. The focus of the surface, airborne, and satellite studies during MAST was to improve the characterization of aerosol microphysical properties and cloud dynamic processes in ship tracks (MAST 1994).

Only a few studies of the in situ characteristics of ship tracks have been carried out. In studies to date, emphasis has been on the aerosol microphysical characteristics of ship tracks (Ackerman et al. 1993; Albrecht et al. 1989; Radke et al. 1989; Ferek et al. 1998), while cloud dynamic aspects have been largely ignored. This is due to the subtle boundary layer cloud perturbations that may trigger ship tracks and the difficulty in measuring these perturbations. The marine environment associated with ship tracks represents extremes with respect to low concentrations of cloud condensation nuclei (CCN) and the lack of surface temperature and roughness differences associated with convective turbulence effects in clouds. Numerical models that go beyond most plume rise and dispersion models can be useful in understanding the sensitivity of marine stratiform clouds to CCN and turbulence effects. Innis et al. (1998, manuscript submitted to *J. Atmos. Sci.*) calculate that temperature differences as small as 0.1°C can increase cloud-level aerosol concentrations by over a factor of 2 in decoupled boundary layer conditions. Systematic vertical velocities as low as a few centimeters per second and/or associated air temperature increases of less than 1 K have produced modifications of marine boundary layer clouds in a statistical–dynamic numerical model that mimic many of the morphological and cloud liquid water characteristics associated with ship tracks (Porch et al. 1990).

Important measurements were made during the MAST experiment from the R/V *Glorita.* Vertical profiles of background meteorological parameters (needed as input to numerical models simulating ship tracks) were obtained from both rawinsonde and tethered bal-

Corresponding author address: William M. Porch, Atmospheric Physicist, D-407, Los Alamos National Laboratory, Los Alamos, NM 87545.
E-mail: wporch@lanl.gov

loons launched from the R/V *Glorita* (Syrett 1994). Also, surface properties such as sea surface temperatures and heat and moisture fluxes were obtained from measurements on the ship. Surface aerosol properties and lidar measurements of the interaction of ship plumes and marine boundary layer clouds were made from the ship (Hooper and James 1998, manuscript submitted to *J. Atmos. Sci.*). Measurements of cloud bottom heights related to ship-track clouds were measured from the ship with commercial ceilometers.

Research vessel–based measurements of atmospheric parameters associated with ship tracks have several advantages over aircraft measurements, such as the research vessel being stationed for long periods at sea. Consequently, data were obtained on the evolution of conditions leading to ship-track formation during the day and at night. A ship-based experiment, called SEAHUNT, was performed in 1991 off the coast of Southern California and northern Mexico to study ship tracks and other external forcing on marine boundary layer clouds (Hindman et al. 1994). This experiment documented the first surface observation of a ship-track cloud that was known to be a ship-track cloud simultaneously observed by satellite.

In this paper, we report on the in situ and remote measurement system results aboard the R/V *Glorita* during the MAST experiment. Data from these sensors are combined to characterize the physical and dynamic structure of ambient and ship-affected clouds.

2. Ship-based measurements during MAST

The most important component of the ship-based measurements in MAST was the research ship and its deployment with respect to dedicated navy ships and ships of opportunity that affected marine stratiform clouds during MAST. A complete description of the aircraft and ship operations, a description of the physical and power plants including the trajectory of each of the dedicated ships, and what is known about the ships of opportunity can be found in Gasporivic (1995). In this paper we will focus on the dedicated navy ships USS *Safeguard* and USS *Mt. Vernon*; and on ships of opportunity on 12, 27, and 28 June when ship tracks and clouds that had been affected by ships that passed over the research vessel. Figure 1 shows the ship tracks as detected in the National Oceanic and Atmospheric Administration/Advanced Very High Resolution Radiometer (NOAA/AVHRR) channel 3 satellite images for these three days. An overview of information on the ships that produced many of the features in Fig. 1 are given in Table 1. These ships varied in fuel type and amount consumed from diesel, steam turbine, and nuclear. The nuclear ship, USS *Truxton*, and the steam turbine, USS *Mount Vernon*, did not produce a ship track. The relatively small USS *Safeguard* diesel ship did make a ship track. The boundary layer depth was about 300 m in the case of the USS *Safeguard* compared to about 500 m in the case of the USS *Truxton* and USS *Mount Vernon*. Larger diesel ships within a few hundred kilometers of the USS *Truxton* and USS *Mount Vernon* did make a visible ship track. More detailed information on these ships and their emissions is given by Hobbs et al. (1998, manuscript submitted to *J. Atmos. Sci.*).

The instruments aboard the R/V *Glorita* consisted of shipborne and balloon-borne sensors (Table 2). Shipborne acoustic, optical, and microwave sensors probed the boundary layer far from the influence of the ship and high surface winds. In situ shipborne measurement systems included a tower for measuring heat and water vapor fluxes, coupled with a floating sea surface temperature measuring device, plus visible and infrared radiometry operated by the NOAA Environmental Research Laboratories (ERL) (Fairall et al. 1997). The tower was located near the bow of the ship and was about 6 m above the deck (10 m above sea level) to avoid as much as possible the effect of the ship's air wake. The instrumentation included global positioning system (GPS) position detection and mast motion sensors to account for translation and rotation effects on the horizontal wind and vertical velocities needed for eddy correlation and estimates of bulk heat and water vapor fluxes.

In situ measurements of aerosol characteristics were made using a sampling on the ship's mast connected to instrumentation in a cabin 20 m below. In situ measurements of aerosol characteristics were made using a 5-cm-diameter sampling tube 6 m up the ship's mast connected to instrumentation in a cabin 14 m below. The analysis of the aerosol sampled from the ship's mast included condensation nuclei (CN), CCN, spectra (Hudson and Li 1995), and aerosol size distributions from diffusion battery measurements. A limited number (12) of aerosol filter samples were taken from a sampler attached to the ship's high mast. A nephelometer also was located on the mast.

In situ balloon-borne sensors measured meteorological parameters. These included conventional temperature, humidity, and wind profiling sensors for rawinsonde and tethered balloons. Rawinsondes were launched every 3 h during potential ship track periods.

Active remote sensing instruments included a scanning lidar, which was mainly dedicated to studies of ship plume and background aerosol inhomogeneities and their transport and interaction with boundary layer clouds (Hooper and James 1998, manuscript submitted to *J. Atmos. Sci.*). Two commercial lidar–ceilometers were mounted to the deck for continuous determination of cloud bottom heights and backscatter. The Pennsylvania State University (PSU) system was pointed vertically and the Los Alamos National Laboratory (LANL) system was oriented 40° from vertical pointing aft of the ship. This was done to increase the path in the boundary layer for increased aerosol sensitivity and to improve resolution of cloud edges during cloud openings. A Doppler acoustic sounder (Porch et al. 1988)

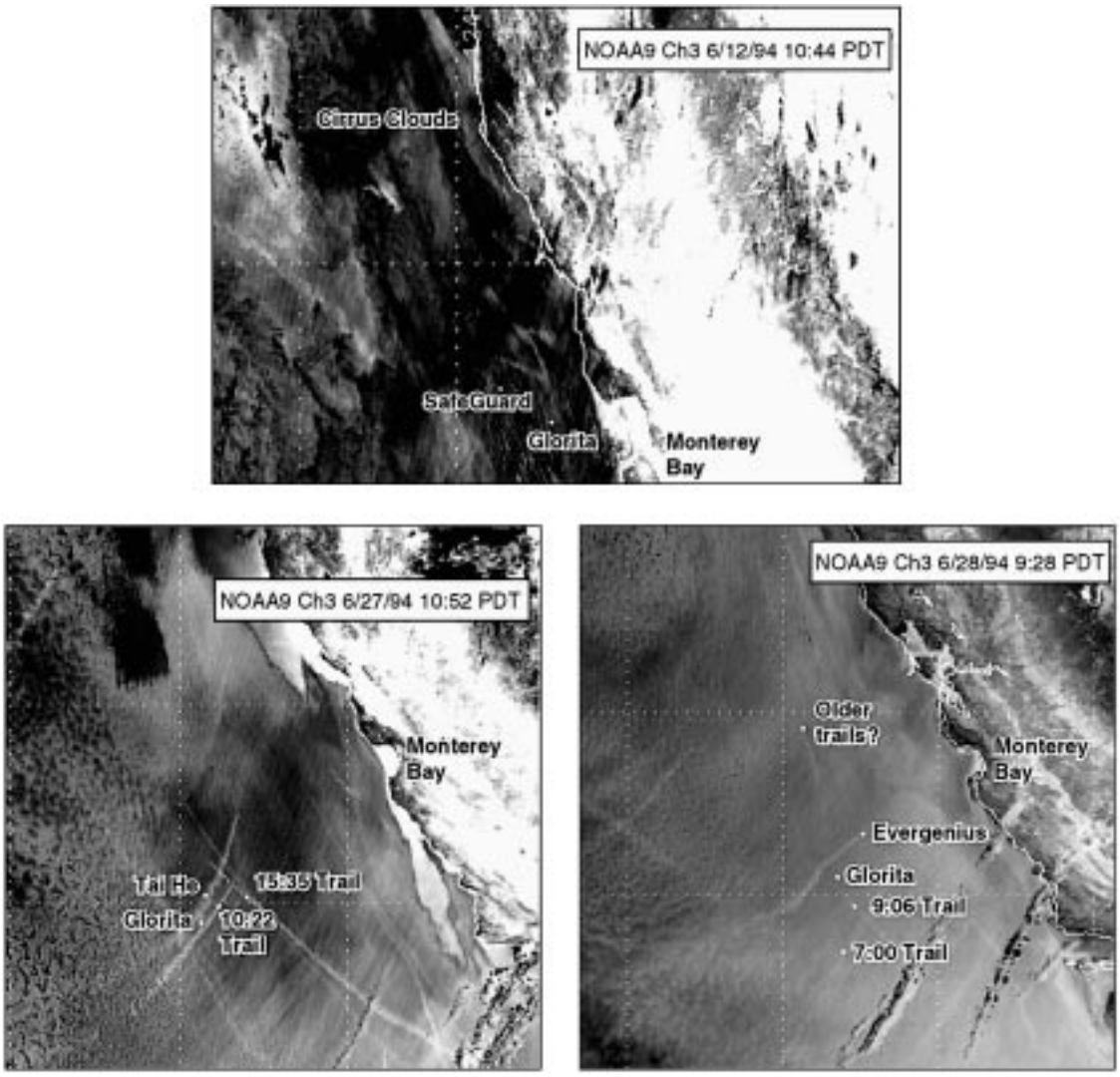

FIG. 1. NOAA AVHRR satellite images on 12, 27, and 28 June 1994 showing locations of R/V *Glorita,* dedicated navy ships, and ship tracks. These experiments were conducted 100–200 km west of Monterey Bay, CA. The dark features on 12 June are associated with cirrus clouds that were tending to mask the ship tracks on this day. The ship track from the USS *Safeguard* on 12 June was directly related to the navy ship and showed strong effects on the overlaying cloud morphology. On 27 June three prominent older ship tracks were observed that displayed smaller morphological effects. On 28 June the ship tracks were not as bright and were associated with larger commercial vessels rather than dedicated navy ships that used steam turbine and nuclear power sources.

TABLE 1. Ship characteristics.

Ship	Propulsion	Plume heat (MW)*	Speed (kt)	Length (m)− displacement (kg × 10^6)
USS *Safeguard*	Diesel 4200 hp	1.6	14	77.7 − 2.6
USS *Mount Vernon*	Steam turbine 24 000 hp	8.9 (Steam)	22	168.6 − 12.4
USS *Truxton*	Nuclear 70 000 hp	(Water cooled)	30	171.9 − 8.3
Tai Hi	Diesel 22 088 hp	8.2	19	231.6 − 32.6
Evergreen *Evergenius*	Diesel 21 600 hp	8.1	20.5	230.8 − 33.5

* Assuming 50% efficiency.

TABLE 2. Specifications of instruments used on the R/V *Glorita.*

Instrument system	Parameters	Source	Accuracy (±)	Precision (±)*
Meteorological				
Ceilometer (LANL)	Cloud base height	Handar	15 m	N/S
Ceilometer (PSU)	Cloud base height	Väisälä	15 m	N/S
Cloud video (time lapsed)	Cloud field images	LANL	N/S	N/S
Doppler radar	Radar return	LANL	N/S	N/S
(LANL) 35 GHz	Vertical velocity		5 cm s^{-1}	1 cm s^{-1}
Doppler radar (PSU) 94 GHz	Radar return	PSU	0.2 dB/MSD	0.2 dB/MSD
Doppler sodar	Horizontal, vertical velocity and C_T^2 profiles	Remtech	0.2 m s^{-1}	0.1 m s^{-1}
			5 cm s^{-1}	1 cm s^{-1}
			N/S	N/S
Flux tower (NOAA)	Wind, temperature, and heat flux**	NOAA	0.2 m s^{-1}	N/S
			0.1°C	N/S
			10 W m^{-2}	N/S
Lidar (Nd:YAG)	Elastic aerosol backscattering profiles at 1.06 μm	NRL	N/S	7.5 m
Microwave radiometer	Vertically integrated water vapor and liquid water path	PSU	0.13 cm	0.06 cm
			40.7 μm	14.7 μm
Pyranometer (LANL)	Global solar radiation	LiCor	10 W m^{-2}	1 W m^{-2}
Pyranometer (NOAA)	Global solar radiation	Eppley	5 W m^{-2}	0.5 W m^{-2}
Rawinsonde	Temperature, wind, and humidity profiles	Väisälä	0.2°C	0.1°C
			0.5 m s^{-1}	0.2 m s^{-1}
			3% RH	1% RH
Sea surface temperature sensor	Temperature	NOAA	0.2°C	0.1°C
Tethersonde	Temperature, wind, and humidity profiles	AIR	0.5°C	0.05°C
			0.25 m s^{-1}	0.1 m s^{-1}
			5%RH	0.1% RH
Aerosol				
CN counter	Condensation nucleii	TSI	10 cm^{-3}	1 cm^{-3}
CCN spectrometer	Cloud condensation nuclei vs supersaturation	Desert Research Institute	10 cm^{-3}	1 cm^{-3}
			0.02% SS	0.01% SS
Nephelometer	Light scattering coefficient	Radiance Engineering	2×10^{-5} m^{-1}	1×10^{-5} m^{-1}

* Accuracy is based on estimates of variability of calibration vs a standard, while precision is based on the resolution of the variation.
** For more details, see Fairall et al. (1996).
N/S is not specified.
RH is relative humidity.
SS is supersaturation.

was used for profiling wind, vertical velocity, and boundary layer heights. This system could only be operated during rare periods of calm sea conditions (three days) because internal software disallowed data that displayed too much variability. During calm periods, the sounder was able to track wind speeds and vertical velocities to about 700 m above the instrument. Two Doppler radars were aboard the ship. The PSU system was a high-power pulsed system with a frequency of 94 GHz. The LANL system was a small, battery-operated, continuous wave (CW) system with a frequency of 35 GHz that was gimbaled to compensate partially for ship motions. This system provided only integrated velocity and return signal strength analysis.

Passive remote sensing instruments included a microwave radiometer (used to determine vertically integrated water vapor and cloud liquid water content), two pyranometers, and a pyrgeometer. A whole-sky camera and time-lapse video system provided a continuous record of cloud cover during the day.

3. Results

a. Meteorological profiles

Some of the most important measurements needed for the dynamic modeling of ship-track clouds are temperature and humidity profiles. These were obtained on a regular basis from rawinsonde launches from the ship (every 3 h during cloudy periods). Table 3 summarizes the general sky conditions, whether a ship track was observed within about 500 km of the R/V *Glorita*, and an estimate of the marine boundary layer depth. The marine boundary layer depth often lifted considerably through the day as weather systems passed, and at times as coastal processes affected the boundary layer.

TABLE 3. Sky, ship track, and marine boundary layer depth estimates based on rawinsonde launches from the R/V *Glorita* (usually at 3–h intervals when clouds were present).

Date (June 1994)	Sky conditions	Ship tracks	Boundary layer depth (m)
6	Clear	No	500–1200
8	Low clouds	Yes	150–250
10	Fog	No data	50–200
11	Low clouds	Yes	200–450
12	Low clouds	Yes	350–400
13	Low clouds	Yes	300–700
14	Clear	No	450–650
15	Clear	No	550–650
16	Low clouds	No	600–1300
17	Low clouds	No	700–1300
20	Low clouds	No	600–700
21	Low clouds	No	350–600
22	Low clouds	No	400–650
23	Clear	No	200–500
26	Clear	No	200–450
27	Low clouds	Yes	350–600
28	Low clouds	Yes	500–600
29	Low clouds	Yes	400–500

Table 3 shows that boundary layer depths less than about 500 m were most conducive to ship-track observation. However, there were cases when the boundary layer depths were close to 500 m and no ship tracks were observed near the R/V *Glorita* (e.g., 21–22 June). Boundary layer depth is not the sole condition for ship-track observation. The population of ships in the vicinity large enough or dirty enough to make a ship track is also important. A satellite survey conducted by Coakley et al. (1998, manuscript submitted to *J. Atmos. Sci.*) documents the importance of cloud height to the observation of ship tracks during MAST.

On four days during the MAST experimental period, the winds were low enough to permit tethered balloon launches from the ship for comparison with the rawinsonde profiles. We were able to profile continuously from about 1100 to 1600 PDT 11 June. About five ship tracks were observed in the AVHRR satellite image on this day in clouds similar to those observed near the ship. Unfortunately, none passed over the R/V *Glorita*. Figure 2 shows the short-term effect of a fast (15 min) change in boundary layer height associated with an approaching front and a change from a southerly to northerly wind. This event followed a coastal surge the previous day (Nuss 1995). A coastal surge is a phenomenon observed by satellites reflecting the rapid movement of stratiform clouds up the coast of California. The associated changes in these clouds affected the conditions under which ship tracks were observed during this period. The rawinsonde profiles are included in Fig. 2 for comparison. These show a similar change in boundary layer depth after 1300 PDT but with considerably less vertical resolution than the tethered balloon measurements.

b. Surface conditions

Table 4 shows the surface conditions combined with profile parameters for the periods during three days (with specified time periods) when ship tracks (observable by satellite) and ship-affected clouds (observable effects only from the surface) were observed passing over the R/V *Glorita.* The surface conditions include data taken from the bow-mounted meteorological tower, sea surface temperature probe, and CN measurements. All the data from the meteorological tower were corrected for ship-relative motion. The latent and sensible heat flux estimates are based on mean values of covariance, inertial dissipation, and bulk flux estimates (Fairall et al. 1996). The accuracy of these flux measurements of about ± 10 W m^{-2} must be considered in the context of these mean fluxes and the importance of surface fluxes in numerical stratiform cloud models. The solar radiation data were derived from a diffusing-disk pyranometer. The exposure for this instrument was not ideal, so the absolute irradiance is suspect (the primary radiation sensing system was destroyed early in the experiment during high seas).

Lidar measurements, scanning in both the horizontal and vertical, were used to describe the three-dimensional ship plume evolution from the ship into the marine boundary layer clouds. Figure 3 shows an example of this analysis for the USS *Truxton* plume on 28 June 1994. The USS *Truxton* was a nuclear-powered ship so the measured plume was a combination of small shipboard effluents and sea spray generated by the ship's motion through the ocean. One of the important results of this analysis is that the plume rise was not continuous but was strongly affected by convective elements that are associated with the marine stratus clouds above. This observation shows that overlaying clouds can affect plume dispersal and entrainment of the plume into the clouds. Most of the plume rise seems to occur in regions where the surface level horizontal scan shows relative minima in aerosol backscatter, indicating that the dynamics of the clouds affect the entrainment of the aerosol below. Details of plume rise times and diffusion are described in Hooper and James (1998, manuscript submitted to *J. Atmos. Sci.*). On days when there were no overlaying clouds, the plume rise was more continuous. The cloud convection is a balance of radiative cloud-top cooling, latent heat release in cloud formation, and surface heating.

c. Cloud morphology and dynamics

The properties of clouds affected by ships were remotely sensed with the ceilometers and Doppler radars. Figure 4 shows the raw return signal for the tilted ceilometer during the periods that ship tracks passed overhead of the R/V *Glorita* on 12, 27, and 28 June. The ceilometer laser could not penetrate most of the clouds observed so only the cloud bottoms (shown in white)

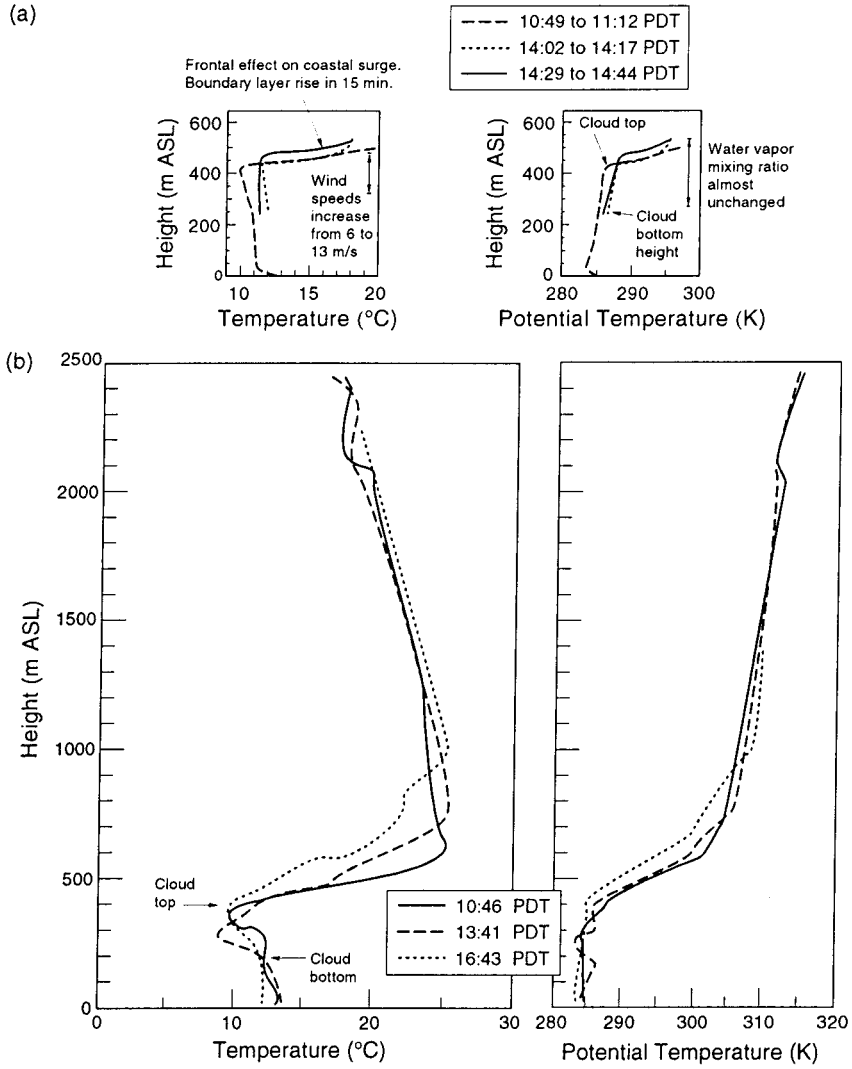

FIG. 2. Comparison of (a) tethersonde and (b) rawinsonde profiles during a coastal wind surge on 11 June 1994. This figure shows the rapid change in boundary layer structure and the extremely low cloud layer associated with the coastal surge and interaction with a moving front.

are quantitative. The top of the white regions are more a measure of the optical depth in the cloud rather than the cloud-top heights. Relatively strong effects on cloud morphology were detected on 12 June, with weaker changes associated with ship-affected clouds the other two days. Most of the changes are associated with the base of the clouds. The bottoms were lower by about 50 m than the background clouds. This condition has characteristics similar to the interaction of cooling tower plumes with overlaying clouds over land. On the other hand, two cases on 27 June seem to show a slightly raised cloud bottom (about 20 m) associated with older tracks (the *Tai He* at about 1100 and an older track at 1540 PDT). Supporting pyranometer data are also shown in Fig. 4. The pyranometer data generally show a relative decrease in solar radiation associated with the ship track and often regions of relatively stronger solar radiation at the sides of the ship track (especially on 12 June).

The changes in cloud base features may be due to either cloud dynamic or cloud droplet microphysics. Adiabatic cooling, either from the initial convective plume from the ship or from evolved dynamic convection in the ship track, could explain the lowering of cloud-base height associated with the ship track. Dynamic effects are consistent with the thinner cloud regions at the sides of ship tracks if general lofting in the ship track is compensated for by subsidence at the edges. It is also possible that the lower parts of the cloud are related to drizzle. However, this would require drizzle production rather than suppression associated with the ship tracks that showed a cloud-base lowering.

The small rises in cloud-base heights in the ship tracks on 27 June is a more subtle effect than the lowered

TABLE 4. General conditions during periods of ship-track passes over research vessel or ship-modified cloud observations.

Parameters (units)	12 Jun 1994 (1300–1800 PDT)	27 Jun 1994 (1030–1430 PDT)	28 Jun 1994 (0630–1300 PDT)
Wind speed at 10 m (m s^{-1})	9.7	9.6	8.9
Wind direction (degrees from true N)	315	343	347
Sea surface temperature (°C)	14.6	15.6	14.8
Air temperature at about 10 m (°C)	13.7	15.3	14.5
Specific humidity at about 10 m (g kg^{-1})	9.1	9.1	9.0
Sensible heat flux (W m^{-2})	16.5	11.7	12.3
Latent heat flux (W m^{-2})	28.2	51.6	11.6
Boundary layer depth (m)	400	600	550
Boundary layer potential lapse rate (°C km^{-1})	2	1	1
Cloud base height (m)	180[a]	430[b]	330[a]
Solar radiation (W m^{-2})	700 [1300–1500]	300–500[b]	100–400[b]
[Times PDT]	300 [1500–1800]	[1000–1400]	[0830–1100]
Condensation nuclei (cm^{-3})	1150	1000	620
Background	1100[c]	500	420
Ship plume	1500–10 000	900–1000	620–4800

[a] Lowering values throughout period.
[b] Rising values throughout period.
[c] Probable contamination of sampling line.

cloud base observed near the origin of the ship track. Analysis from a three-dimensional statistical dynamic stratiform cloud model (Porch and Kao 1996) indicates that once ship tracks are formed the combination of cloud radiative effects and the latent heat released as the cloud develops causes the cloud bottom height to gradually rise with time. The ship tracks observed on 27 June were more mature than the second ship-affected cloud on 12 June (1444–1504 PDT associated with the USS *Safeguard*). However, the ship track feature starting at 1206 PDT 28 June showed raised clouds only at the edges, and the track associated with the *Evergreen Evergenius* on 28 June showed only a slight rise in the center. Each of these clouds seemed as mature as the two tracks with raised cloud bases on 28 June. The pyranometer data show a 30% or greater insolation on

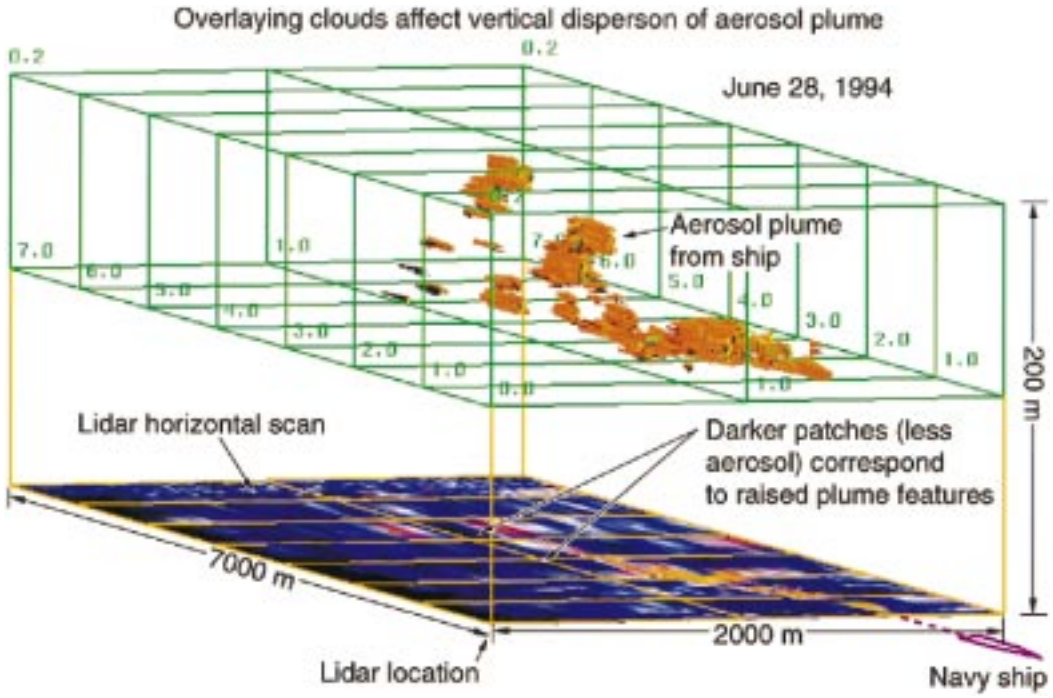

FIG. 3. Lidar image showing ship-effluent intermittent transport to cloud layer above the ship (28 June 1994). The discontinuous plume elements and the correspondence of clearer regions in the horizontal scan below the raised plume features demonstrates the involvement of the plume with active connective elements in the cloud layer above the plume.

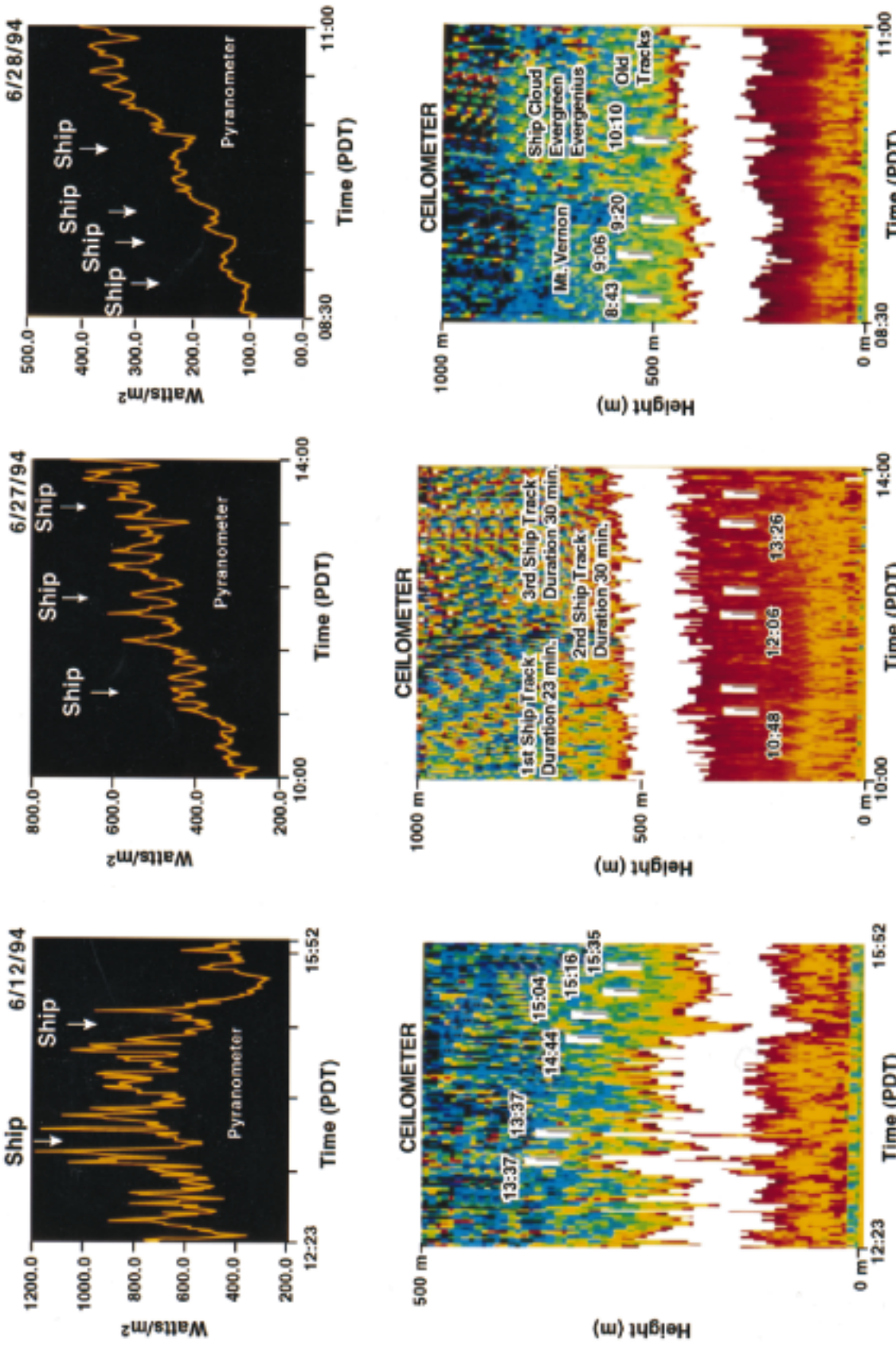

FIG. 4. Ceilometer raw backscatter data arbitrarily scaled backscatter units in [10 000 sr km]$^{-1}$ for 12, 27, and 28 June 1994 and pyranometer comparison. White corresponds to the highest backscattering values (cloud), followed by red (increased aerosol and virga), followed by yellow (boundary layer), and blue (background). When the ship tracks are fresher and the cloud bottoms are lower (12 and 28 June), the ship track cloud is lower than background clouds. When the clouds are higher and older, the track features are higher than the background clouds (27 June).

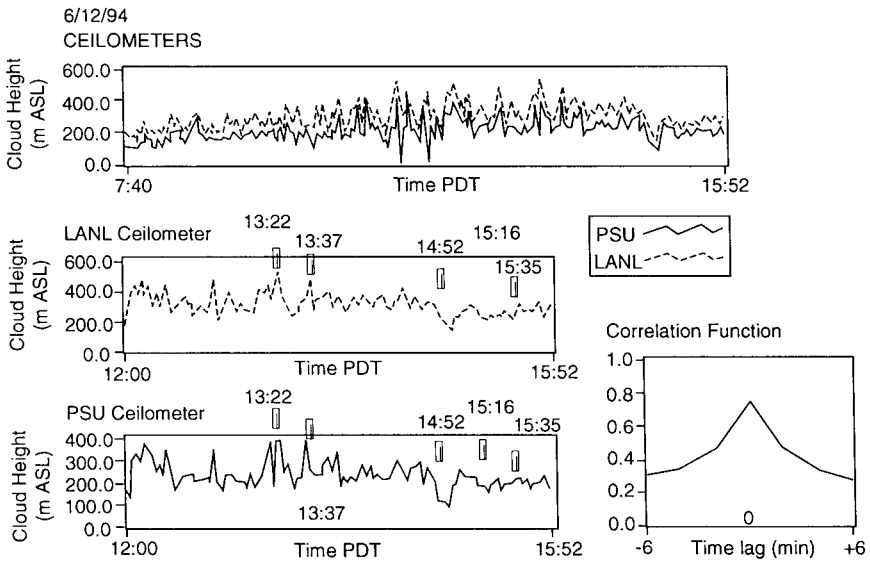

FIG. 5. Processed cloud-ceiling comparison from two ceilometers on 12 June 1994. The PSU ceilometer was oriented vertically, while the LANL system was tilted at 45°. This accounts for the height differences and time-lagged correlation.

12 June than on 27–28 June. The insolation variability is also greater, and the clouds were less dense and more variable on 12 June. The greater insolation implies a greater surface heat flux, which is supported in Table 4.

To check whether the features shown in Fig. 4 may have been due to instrument artifacts, comparisons were performed between the processed cloud heights from the PSU and LANL ceilometers; one such comparison is shown in Fig. 5. As expected, the tilted ceilometer (LANL) shows a higher cloud-base height than the vertically pointed system (PSU). A time lag is introduced because the two ceilometers pointed at regions of the sky separated by about 300 m on 12 June and by about 500 m on 27 June (about the boundary layer height). On 12 June the lag peaks at about 1 min with a correlation greater than 0.8. On 27 and 28 June the correlation was about the same (0.8), with time lags as long as 3 min. Both systems show drops in the cloud-base heights associated with ship tracks and thinner cloud regions on both sides of the tracks. The drop in cloud bottom height associated with the first cloud feature beginning at 1322 PDT is not as great in the processed cloud height data as in the raw data shown in Fig. 4. This implies that this feature, as well as many others on subsequent days, represented a relatively thin cloud. This is consistent with visual observations that the ship-track feature at 1322 PDT had thin scudlike clouds below the main cloud that were not associated with background cloud features.

The two Doppler radars also remotely sensed characteristics of the ship tracks. Figure 6 shows an example of the data from the PSU system on 28 June. In general, when peaks in CN indicated ship plumes below ship-affected clouds these peaks seemed to be associated with stronger radar returns. However, the crossing of the *Mt. Vernon* plume around 0845 PDT showed no peak in CN and was associated with a decrease in radar return (possibly drizzle suppression). The lack of a peak in CN implies that at this measurement point the ship plume did not mix down to the sea surface. The lack of a CN peak makes this event difficult to time precisely. This crossing was also complicated by a ship-track crossing at about 0906 PDT. At times (but not always) the top of the clouds were slightly raised during the periods affected by ships. This is consistent with visual observations of a ship-track cloud extending higher than background clouds during the SEAHUNT experiment (Porch et al. 1996) and the *Sanko Peace* ship track observed during MAST (Durkee et al. 1998, manuscript submitted to *J. Atmos. Sci.*).

Figure 7 shows an example of the LANL CW Doppler radar data for the second ship-affected cloud feature (USS *Safeguard*) at 1444–1504 PDT 12 June. Data storage capacity limited the observation periods for this instrument to about 1 h. This figure compares the radar return strength (arbitrary units), the integrated Doppler vertical velocity (compensated for ship and horizontal cloud motion), the liquid water path from the microwave radiometer, the pyranometer signal (compensated for sun angle), and the ceilometer estimated cloud height. The CN measurements showed a very strong plume associated with this feature with CN concentrations rising to a maximum of about 10 000 cm^{-3}. Concentrations outside the plume were in the range of 1000 cm^{-3} (this was a very clean day, as observed by aircraft measurements and may indicate some sample contamination in this case). The remote sensing comparison in Fig. 7 shows that there is an apparent correspondence between

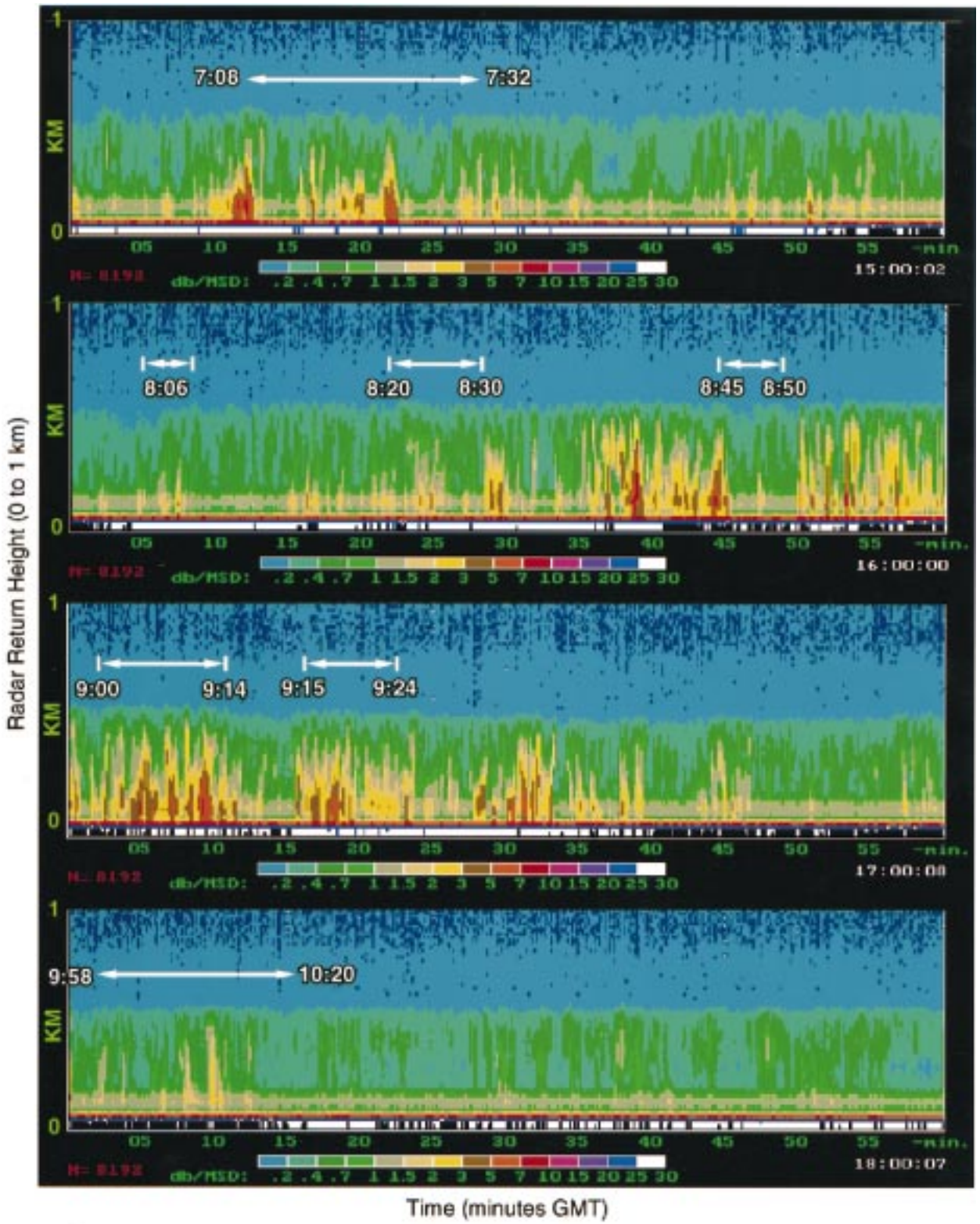

FIG. 6. The Pennsylvania State University Doppler radar reflectivities on 28 June 1994 to a height of 1 km above the sea surface. The highlighted times correspond to the ship-affected cloud observations shown in Table 5. This figure shows the variability of cloud radar reflectivities on 28 June and the lack of definite relationship between ship tracks (with associated increases in optical reflectivities) and decreased cloud radar reflectivities (actually, the reflectivities seemed to be larger except for the 0845–0850 PDT) expected if drizzle-sized droplets are diminished.

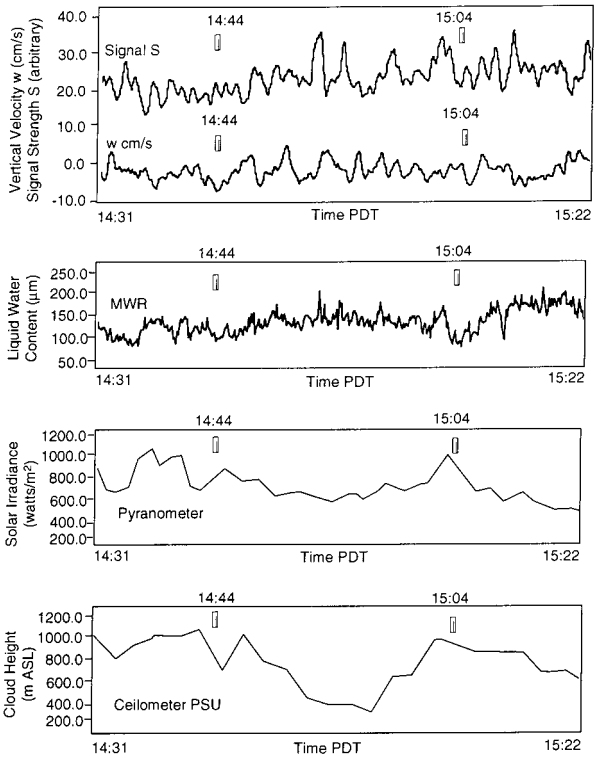

FIG. 7. LANL Doppler radar, MWR, and pyranometer comparison for 12 June 1994. The vertical bars bound the ship plumes as detected in the CN data. These comparisons show the higher radar signal level and slightly increased vertical velocities from the Doppler radar and associated higher liquid water content from the microwave radiometer, decreased solar irradiance, and cloud bottom height associated with the smaller ship-track feature shown in Fig. 4 for 12 June.

the radar return strength and the cloud liquid water. Also, where the cloud liquid water is reduced at the sides of the feature, the Doppler vertical velocities show small peaks in subsidence. The transparency of the cloud, as shown by the pyranometer, peaks when the cloud liquid water decreases at the sides of the feature; the subsidence is maximized and the cloud bottom height reaches its relative maximum.

The ship track events on 12 June are the best example obtained during MAST of comparisons between the ship-based measurements during a ship-affected cloud event. However, most of the features were observed at other times, although more subtly. Table 5 generalizes the comparisons for the ship-track and ship-affected cloud situations we have been able to identify for 28 June. The CN concentrations at the surface were much lower during the two ship-track passes on 28 June than on 12 June, reflecting the close location of the USS *Safeguard* on the 12th and the greater age of the ship tracks on the 28th.

Table 5 shows the variability of characteristics observed from the ship of ship-affected clouds. The general separation of ship-track and ship-affected clouds comes from the fact that cloud effects were observed from the ship that did not correspond to a satellite-observed ship track. This is due either to a timing difference between the satellite images and ship overpass or the feature was too small or too weak at cloud top to be resolved by satellite. Although, in general, these features were associated with increases in CN at ship level, this was not always the case. Many of the features showed decreases in pyranometer signal and increases in liquid water content and radar reflectivity, but again this was not always the case. As discussed previously, although the younger ship tracks and ship-affected cloud features usually demonstrated a slight lowering of cloud base, older ship tracks showed little effect or a slight rise. In spite of the small contribution of surface effects in generating convective turbulence in marine stratiform clouds, convective elements develop in these clouds and ship tracks embedded in them. This affects the measurements made in each pass underneath them at the surface by a ship as well as aircraft passes through them. These convective elements are associated with cloud microphysics, cloud morphology, and CCN concentrations. Taken together, these data only suggest occasional dynamic and microphysical effects of ships on clouds. More measurements are needed to provide a robust statistical description of ship-track characteristics.

4. Conclusions

Ship-based measurements provided unique information related to ship-track clouds from surface measurements and meteorological profiles from tethered and free balloons. The data are critical as inputs to, and constraints on, numerical models designed to simulate the effects of ship-plume aerosols, heat and moisture, and ship air wakes on marine stratiform clouds. Aerosol measurements of CN at ship-mast-level identified ship plumes. Lidar backscattering images showed ship plumes couple with convective elements in overlaying cloud layers.

Information was obtained on cloud morphological changes associated with ship tracks. Comparison of data from remote sensors aboard the ship shows that ships often affected the base and top heights of clouds. Comparison of data from remote sensors aboard the ship shows that ships often affected the base and top heights of clouds by as much as 50–100 m. Relatively strong effects on cloud morphology were detected on 12 June, showing a drop in cloud base of 100 m in a freshly produced ship track. Pyranometer measurements showed increased solar irradiance values of about 400 W m^{-2} on both sides of the ship track. Also, ship-affected clouds often have thin cloud or cloud-free regions on their sides. These physical features indicate that cloud dynamics may often be an impor-

TABLE 5. Measurement comparisons during ship-affected cloud events on 28 Jun 1994.

Event	Times (PDT)	Satellite	CN (cm^{-3})	Ceilometers	PSU radar	LANL radar	MWR	Pyranometer
Weak track	0708–0736	N12ch3* 1052 image	No data	Variable ceiling drops 50 m drops at sides 0708 and 0736	Period of relatively strong returns	No data	LWC high with decrease in middle, dips at 0708 and 0736	Low light with small peaks at 0708 and 0736
Weak ship cloud effect *Mt. Vernon*	0806	Not visible	Short peak 0806	Very slight dip 20 m at 0802	Very weak increase 0806	No data	No effect	Very small peak
Weak ship cloud effect *Mt. Vernon*	0820–0830	No visible on N12ch3 image	Short peak CN 4800 $cm^{-3;}$ background 420 cm^{-3} 0820–0830	No or very weak dip 10 m at 0826	Period of stronger returns 0823–0830 with decrease at 0826–0828	No data	Noticeable peak in LWC with dips at edges at 0826 and 0830	Peaks at edges 0826 and 0830 Slight decrease in center 0828
Weak ship cloud effect (hard to time; no CN peak) *Mt. Vernon*	0845–0850	Not visible	No peak	Slight dip 25 m about 0845	Period of strong returns from 0835–0845, weak from 0845–0855 (drizzle suppression?)	No data	Increase in LWC before/after 0845, decrease 0845–0850	Slight or no decrease through period
Ship track	0906–0914 ±5 min	2d Ship track N 12ch3 0928 image	Short peak 0906–0910 CN 620 cm^{-3}	Strong dip 20–40 m at 0906	Period of strong returns 0850–0910 decrease at 0902	No data	Small increase with decreases at 0900 and 0910	Decrease with small peaks at 0900 and 0915
Weak ship cloud effect *Mt. Vernon*	0915–0924	Not visible	No data	Slight dip 20 m	Period of strong returns 0915–0924	No data	No effect	Small decrease with peaks at 0915 and 0924
Ship Track *Evergreen Evergenius*	0952–1007 (±14 min)	Strong N12ch3 1052 image	No data	Dips on each side (20 m) Stronger signal in raw data 0958–1020	Weak signal increase 0957–1012	No observable signal increase Slight increase in subsidence (5 cm s^{-1}) 1020	Slight increase in LWC with dip at 1020	Little effect peaks at 1020 and 1050
Older track?	1050–1120	Only first part visible N12ch3 1052 image	No peaks	Strong dips in raw data, only one dip in ceiling 50 m at 1052	No observable effect	Strong subsidence peaks–25 cm s^{-1} 1050, 1113, and 1120	Very slight decrease in LWC	No observable effect

* N12ch3 is NOAA AVHRR 9 Channel 3.

tant component of ship-track features. These features, combined with the fact that ship tracks seem to occur only within a relatively narrow range of boundary layer depths (about 0–600 m; Durkee et al. 1998, manuscript submitted to *J. Atmos. Sci.*), present a challenge to numerical modeling of ship tracks. The possibility that cloud droplet distributions may differ with height in ship-track clouds compared to background clouds due to internal dynamics present a challenge to the interpretation of aircraft measurements of aerosol and droplet spectra.

Acknowledgments. This work was performed under support from the Department of Defense, Office of Naval Research Grant N00014-94-1-0681, and the Department of Energy, Office of Health, and Environmental Research Grant KP-01. The authors would like to thank J. Archuleta, M. Buchwald, P. Hobbs, L. May, T. Najita, W. Shaffer, W. Spurgeon, B. Albrecht, D. Babb, C. Fairall, J. Hudson, G. Demme, D. Kaplan, M. Miller, and the captain and crew of the R/V *Glorita*.

REFERENCES

Ackerman, A. S., O. B. Toon, and P. V. Hobbs, 1993: Dissipation of marine stratiform clouds and collapse of the marine boundary layer due to depletion of cloud condensation nuclei by clouds. *Science,* **262,** 226–228.

Albrecht, B. A., 1989: Aerosols, cloud microphysics, and fractional cloudiness. *Science,* **245,** 1227–1230.

Conover, J. H., 1966: Anomalous cloud lines. *J. Atmos. Sci.,* **23,** 778–785.

Fairall, C. W., E. F. Bradley, D. P. Rogers, J. B. Edson, and G. S. Young, 1996: Bulk parameterization of air–sea fluxes for Tropical Ocean–Global Atmosphere Coupled Ocean–Atmosphere Response Experiment. *J. Geophys. Res.,* **101,** 3747–3764.

——, A. B. White, J. B. Edson, and J. E. Hare, 1997: Integrated shipboard measurements of the marine boundary layer. *J. Oceanic Atmos. Technol.,* **14,** 368–379.

Ferek, R. J., D. A. Hegg, P. V. Hobbs, P. Durkee, and K. Nielsen, 1998: Measurement of ship-induced cloud tracks off the Washington coast. *J. Geophys. Res.,* in press.

Gasparovic, R. F., 1995: *MAST Experiment Operations Summary*. The Johns Hopkins University Applied Physics Laboratory, 295 pp.

Hindman, E. E., W. M. Porch, J. G. Hudson, and P. A. Durkee, 1994: Ship-produced cloud lines of 13 July 1991. *Atmos. Environ.,* **28,** 3393–3403.

Hudson, J. G., and H. Li, 1995: Microphysical contrasts in Atlantic stratus. *J. Atmos. Sci.,* **52,** 3031–3040.

MAST, 1994: Monterey Area Ship Track (MAST) Experiment: Science plan. Naval Postgraduate School Rep., NPS-MR-94-004, 45 pp.

Nuss, W., 1995: NPS Coastal Boundary Layer Experiment 1994. Naval Postgraduate School, 68 pp.

Porch, W. M., and C-Y Kao, 1996: Ocean measurements and models of ship trail cloud characteristics. *Second Int. Conf. on Global Energy and Water Cycle*, Washington, DC, GEWEX, 353–355.

——, W. D. Neff, and C. W. King, 1988: Comparisons of meteorological structure parameters in complex terrain using optical and acoustic techniques. *Appl. Opt.,* **27,** 2222–2228.

——, C.-Y. Kao, and R. G. Kelley, 1990: Ship trails and ship-induced cloud dynamics. *Atmos. Environ.,* **24A,** 1051–1059.

——, ——, M. I. Buchwald, W. P. Unruh, P. A. Durkee, E. E. Hindman, and J. G. Hudson, 1996: The effects of external forcing on the marine boundary layer: Ship trails and a solar eclipse. *Global Atmos. Ocean Syst.,* **3,** 323–340.

Radke, L. F., J. A. Coakley, and M. D. King, 1989: Direct and remote sensing observations of the effects of ships on clouds. *Science*, **246,** 1146–1148.

Syrett, W. J., 1994: Low-Level Temperature and Moisture Structure from the Monterey Area Ship Track Experiment. The Pennsylvania State University, Department of Meteorology, 35 pp.